

Rotation-Invariant Autoencoders for Signals on Spheres

Suhas Lohit

Mitsubishi Electric Research Laboratories
Cambridge, MA

slohit@merl.com

Shubhendu Trivedi

Massachusetts Institute of Technology
Cambridge, MA

shubhendu@csail.mit.edu

Abstract

Omnidirectional images and spherical representations of 3D shapes cannot be processed with conventional 2D convolutional neural networks (CNNs) as the unwrapping leads to large distortion. Using fast implementations of spherical and $SO(3)$ convolutions, researchers have recently developed deep learning methods better suited for classifying spherical images. These newly proposed convolutional layers naturally extend the notion of convolution to functions on the unit sphere S^2 and the group of rotations $SO(3)$ and these layers are equivariant to 3D rotations. In this paper, we consider the problem of unsupervised learning of rotation-invariant representations for spherical images. In particular, we carefully design an autoencoder architecture consisting of S^2 and $SO(3)$ convolutional layers. As 3D rotations are often a nuisance factor, the latent space is constrained to be exactly invariant to these input transformations. As the rotation information is discarded in the latent space, we craft a novel rotation-invariant loss function for training the network. Extensive experiments on multiple datasets demonstrate the usefulness of the learned representations on clustering, retrieval and classification applications.

1. Introduction

Advances in computational imaging and robotics has resulted in an increase in interest in processing spherical/omnidirectional images obtained from 360^0 cameras [44, 13]. As such cameras have been becoming cheaper, they are now part of products such as robots [32], surveillance cameras [31] and “action cameras” such as GoPros. However, conventional deep learning techniques for regular images i.e. 2D convolutional neural networks (CNNs) which are the best performing machine learning methods of today, are not suitable for processing spherical images. This is because, in order to employ the regular 2D CNN, the signal on the sphere must be first unwrapped into a 2D array, which creates a large amount of non-uniform

distortion throughout the image (the topology of S^2 is different from that of \mathbb{R}^2). The same is true for the case of spherical representations of 3D shapes, where the 3D shapes are converted to functions on spheres using ray-casting. This incompatibility between domains necessitates novel designs of neural networks which are tailored to spherical images.

To this end, Cohen et al. [5] and Esteves et al. [10] independently designed convolutional neural networks that can operate directly on signals on spheres. Both these methods involve defining a correlation function between signal on a sphere and a trainable kernel, which is also a signal on the same sphere. This can be achieved computationally efficiently using spherical harmonics. An important feature of this correlation operation is that it is *equivariant* to 3D rotations of the sphere. This is analogous to the usual 2D CNNs for regular images which are equivariant to 2D translations. These spherical convolutional layers can then be stacked along with non-linearities to form deep neural networks for spherical signals. These networks have so far mainly been employed for classification problems where a spherical image is mapped to one of many predefined classes.

All these networks are trained in a supervised fashion, and require a lot of labeled data. In this paper, we propose an unsupervised framework for spherical images. In particular, we design a novel autoencoder architecture such that the latent features remain exactly invariant to any rotation of the input signal. This is because, in many applications, *the inputs do not have a canonical rotation, and the particular orientation that the input signal is measured in is a nuisance factor and should ideally be factored out*. However, as the latent space is rotation-invariant, the usual loss functions cannot be employed for training the proposed autoencoder. Instead, we design a novel loss function, based on the spherical cross-correlation between the estimated output and the desired output, which is also invariant to the relative orientation of the estimated output with respect to the desired output. We now summarize our contributions below.

1. We propose a novel autoencoder architecture for spherical images, where the latent features are guaranteed to be invariant to 3D rotations applied at the input.

2. We carefully design a novel rotation-invariant loss function, based on the maximum value of the spherical cross-correlation between the estimated and desired outputs which is used to train the rotation-invariant spherical autoencoder.
3. We show that the latent features learned using the proposed unsupervised framework are superior to a vanilla autoencoder which does not use the proposed rotation-invariant loss function, for multiple tasks including clustering, retrieval and classification.

2. Related Work

In this section, we briefly review literature related to invariant representations using deep learning and equivariant neural networks. Before that, we define equivariance and invariance with respect to a set of transformations \mathcal{T} . Consider, for simplicity, functions $f, g : L^2(\mathbb{X}) \rightarrow L^2(\mathbb{X})$. For all $x \in \mathbb{X}$, where \mathbb{X} is some space on which the functions are defined. $f(\cdot)$ is invariant with respect to \mathcal{T} if $\forall T \in \mathcal{T}, f \circ T(x) = f(x)$. Similarly, $g(\cdot)$ is equivariant with respect to \mathcal{T} if $\forall T \in \mathcal{T}, g \circ T(x) = T \circ g(x)$.

2.1. Invariant representations using deep learning

While deep learning has produced some very good results for various applications in computer vision, they come at the expense of requiring large amounts of training data and computational resources [23] and a disadvantage that these deep models are often very sensitive to small input variations [7]. At the same time, these overparameterized models are prone to learning mappings that are spurious correlations [2], also known as shortcuts [12]. Goodfellow et al. [14] showed that while regular CNNs do provide some translational invariance, invariance to other transformations cannot be guaranteed. To remedy this drawback, various approaches have been studied in the recent past. These include *hybrid* model- and data-driven approaches such as spatial [16] and temporal transformers [27] which use specially designed modules to model nuisance factors, capsule networks for autoencoding by Hinton et al. [15] and for classification by Sabour et al. [34] which explicitly model pose variations, and other works which modify the convolutional layers for added scale [43] and affine invariances [42]. In the realm of unsupervised representation learning, which is the focus of this paper, several disentangling methods have been proposed. In these methods, the elements of latent vectors are encouraged to represent disentangled factors of variation. That is, if an element of the latent vector, which encodes a particular factor of variation, is removed, the rest of the vector remains invariant to that factor. Examples in computer vision include the works by Kulkarni et al. [24] which disentangles factors of variation for face images, Shukla et al. [37] who propose us-

ing orthogonal latent spaces to encourage disentanglement, Shu et al. [36] and Koneripalli et al. [21] who use spatial and temporal transformer modules in autoencoders in order to encourage affine-invariant representations for images and rate-invariant representations for human motion sequences. Permutation-invariant unsupervised representations for point-clouds has also been effective [1, 45].

2.2. Equivariant neural networks

In addition to the above methods, a new promising class of architectures has emerged which, unlike previous methods, can *guarantee exact invariance* to certain transformations by design. The general architecture is as follows. There is a stack of *equivariant* layers which operate on the input, followed by a pooling/aggregation layer which promotes the representations to be fully invariant. In the case of classification architectures, the invariant features are then passed through the layers of a classifier head.

As mentioned in the introduction, the CNNs used for regular images are equivariant to 2D translations. Cohen and Welling [4] described Group-CNNs which are equivariant to the action of discrete rotations on images. This idea has been applied for autoencoders by Kuzminykh et al. [25]. These ideas were then extended to the case of continuous rotations by Weiler et al. [39] and to both rotations and translations by Worrall et al. [41]. The idea of CNNs have been extended for the case of spherical images by several authors. Kondor and Trivedi [20] showed theoretically that a convolutional structure is actually necessary, and not just sufficient, in order to guarantee equivariance to actions of compact groups on signals. Cohen et al. [5] and Esteves et al. [10] concurrently developed spherical CNNs based on spherical correlation layers, which are computed efficiently using the spherical and SO(3) Fourier transform (SOFT) [22]. Kondor et al. proposed Clebsch-Gordan Nets [18] which operated fully in the Fourier domain and is computationally more efficient. More recently, Esteves et al. [11] designed spin-weighted CNNs which are computationally more efficient compared to [5] and at the same time, do not sacrifice representation power unlike the isotropic filters used in [10]. In this paper, we employ the layers proposed by Cohen et al. [5], however the ideas presented in this paper are applicable to these other architectures as well. Similar ideas have been used to design network layers equivariant to scaling and blurring operators on images [40], rotation equivariance for point clouds [47], learning on sets [33, 46, 30] and graphs [19, 29, 38], gauge equivariant transforms for spheres [3] and meshes [6]. Existing literature on equivariant networks has mainly focused on supervised learning and classification problems. *In this paper, we propose an spherical CNN-based autoencoder for spherical images with a rotation-invariant latent space.* We now describe the background necessary to develop this framework.

3. Background: correlations on S^2 and $SO(3)$

In this section, we provide a brief overview of the mathematical ideas required to define and compute correlations of signals defined on the unit sphere S^2 and the group of 3D rotations $SO(3)$. Please refer to the excellent article by Esteves [9] for a longer treatment of these ideas. Briefly, by the unit sphere S^2 , we mean the set of points $x \in \mathbb{R}^3$ such that $\|x\|_2^2 = 1$. Clearly, this is a 2-dimensional space and can be equipped with a Riemannian manifold structure with the usual inner product as the Riemannian metric. As such, the points on the sphere can be specified using a two-dimensional spherical co-ordinate system say $\alpha \in [0, 2\pi], \beta \in [0, \pi]$. The set of 3D rotations, denoted by $SO(3)$, is a three-dimensional space which can be specified using the popular convention of ZYZ Euler angles given by $\alpha \in [0, 2\pi], \beta \in [0, \pi], \gamma \in [0, 2\pi]$, which quantify the rotation around the Z-, X- and Z- axes respectively performed in order. Note that several such conventions exist and we can easily transform the coordinates from one system to another. Signals/images on S^2 and $SO(3)$ can be described as functions $f : S^2 \rightarrow \mathbb{R}$ and $g : SO(3) \rightarrow \mathbb{R}$ respectively. Note that filters in the layers as well as the output feature maps are such functions.

We can now define a correlation – convolution, in deep learning parlance – between a spherical image f on the sphere with a filter h , which is also a function on the sphere as follows:

$$h \star f(R) = \int_{S^2} h(R^{-1}x)f(x)dx, \quad (1)$$

where \star refers to S^2 correlation, $R \in SO(3)$ is a rotation matrix, dx is a rotation invariant measure of integration given by $d\alpha \sin(\beta)d\beta/4\pi$. Note that (a) by this definition of correlation, the output of the correlation operator for two signals on S^2 is a signal on $SO(3)$. (b) this definition is not unique. Equation (1) is followed in this paper following Cohen et al. [5]. Esteves et al. [10] define a different correlation operator where the output is still a function on S^2 . They show that their definition restricts the filters h in (1), which are eventually learned from data, to be isotropic/zonal filters. This can increase computational efficiency, but at the cost of reduced expressivity.

Similarly, for a function f and a filter h on $SO(3)$, the $SO(3)$ correlation is defined as

$$h \star f(R) = \int_{SO(3)} h(R^{-1}X)f(X)dX, \quad (2)$$

where \star now denotes correlation on $SO(3)$, dX is the measure of integration given in ZYZ Euler angles by $d\alpha \sin(\beta)d\beta d\gamma/8\pi^2$. Note that these definitions of correlations are equivariant to the rotation group $SO(3)$. That is, if the function f undergoes a rotation R , the correlation

output undergoes the same rotation. Please refer Cohen et al. [5] and Kondor et al. [18] for more details.

Now, we discuss how to compute them efficiently using spherical and $SO(3)$ Fourier transforms. We compute the Fourier coefficients for a signal on S^2 by projecting it onto the spherical harmonics, the elements of which are denoted by $Y_m^l(x)$, with two indices: the degree $l \geq 0$ and order m such that $-l \leq m \leq l$. The Fourier coefficients of a bandlimited signal f with a bandwidth of b are thus given by

$$\hat{f}_m^l = \int_{S^2} f(x)\bar{Y}_m^l(x)dx. \quad (3)$$

It also follows that the inverse Fourier transform, i.e., the synthesis function is given by

$$f(x) = \sum_{l=0}^b \sum_{m=-l}^l \hat{f}_m^l Y_m^l(x). \quad (4)$$

Similar to the above, in order to compute the $SO(3)$ Fourier Transform of a signal defined on the group of rotations $SO(3)$, we project it onto the *irreducible representations* of the $SO(3)$ group, which are called Wigner-D matrices, the elements of which are denoted by $D_{m,n}^l$. $D_{m,n}^l$ has a dimension $2l+1 \times 2l+1$ and m, n index the rows and columns of the matrix. The Fourier coefficients of a signal f defined on $SO(3)$ with a bandwidth of b is given by

$$\hat{f}_{m,n}^l = \int_{SO(3)} f(x)\bar{D}_{m,n}^l(x)dx. \quad (5)$$

The inverse $SO(3)$ Fourier transform is given by

$$f(R) = \sum_{l=0}^b (2l+1) \sum_{m=-l}^l \sum_{n=-l}^l \hat{f}_{m,n}^l D_{m,n}^l(R). \quad (6)$$

Now that the required Fourier and inverse Fourier transforms have been defined, we can compute the correlation on S^2 between f and h using the correlation theorem:

$$\widehat{h \star f}^l = \hat{f}^l \hat{h}^{l\dagger}. \quad (7)$$

That is, we first compute the Fourier coefficients \hat{f}^l and \hat{h}^l for $l = 0, \dots, b$, which are vectors. Then we compute the outer product which gives us the Fourier transform of the correlation operator. Finally, we compute the inverse $SO(3)$ Fourier transform which gives us the desired output of the correlation, which is a function on $SO(3)$.

In a similar fashion, we can compute the $SO(3)$ correlation between a function f and a filter h , both defined on $SO(3)$ using a very similar formula as in Equation (7), where we use the forward $SO(3)$ Fourier transform for computing \hat{f} and \hat{h} , which are now block matrices. They are

multiplied together and then we compute the inverse $SO(3)$ transform to yield the correlation output, also on $SO(3)$. In this paper, we use the excellent Pytorch/CUDA implementations of the above functions provided by Cohen et al. [5] for building our framework.

4. Rotation-invariant autoencoder for spherical images

In this section, we describe the proposed autoencoder architecture for signals on spheres, the rotation-invariant latent space, and the novel loss function used to train the network. See Figure 1 for an illustration of the proposed framework.

4.1. Encoder

Given an input spherical image $f^{(0)} : S^2 \rightarrow \mathbb{R}^{C_0}$, where C_0 is the number of channels in the input, it is passed through multiple stacked convolutional layers each followed by non-linearities. This is similar to the usual convolutional encoder for regular images. The first convolutional layer performs a correlation on S^2 , between $f^{(0)}$ and the filters $\{h_i^{(1)}, i=1, \dots, C_1\}$, where $h_i^{(1)} : S^2 \rightarrow \mathbb{R}^{C_0}$. We perform spherical correlation between the input spherical image and the first layer filters, and apply a non-linearity producing the output of the first layer – a signal $f^{(1)} : SO(3) \rightarrow \mathbb{R}^{C_1}$, as explained in Section 3. The rest of the convolutional layers in the encoder are $SO(3)$ correlations where the filters of layer $d, d > 1$, $\{h_i^{(d)}, i = 1, \dots, C_d\}$, where $h_i^{(d)} : SO(3) \rightarrow \mathbb{R}^{C_{d-1}}$. After the input is fed through the D convolutional layers producing the feature map $f^{(D)} : SO(3) \rightarrow \mathbb{R}^{C_D}$. We now use an integration layer to create the rotation-invariant $f_{inv} \in \mathbb{R}^D$ given by

$$f_{inv}(i) = \int_{SO(3)} f_D(X) dX, \quad i = 1, \dots, D. \quad (8)$$

Once we have a rotation-invariant representation, we use further fully connected layers to map to the latent rotation-invariant representation which we denote by $\mathbf{z} \in \mathbb{R}^N$.

4.2. Decoder

The purpose of the decoder is to map the latent representation back to the original input space. To this end, the first layer of the decoder is a fully connected layer that maps \mathbf{z} to a function f on $SO(3)$. We then use a series of $SO(3)$ convolutional layers, similar to those in the encoder, to map to $g : SO(3) \rightarrow \mathbb{R}^{C_0}$. Note that $SO(3)$ correlations produce outputs which are functions on $SO(3)$. In order to construct the desired function on S^2 , we use another integration layer which integrates over γ :

$$\hat{f}(\alpha, \beta) = \int_{\gamma=0}^{2\pi} g(\alpha, \beta, \gamma) d\gamma \quad (9)$$

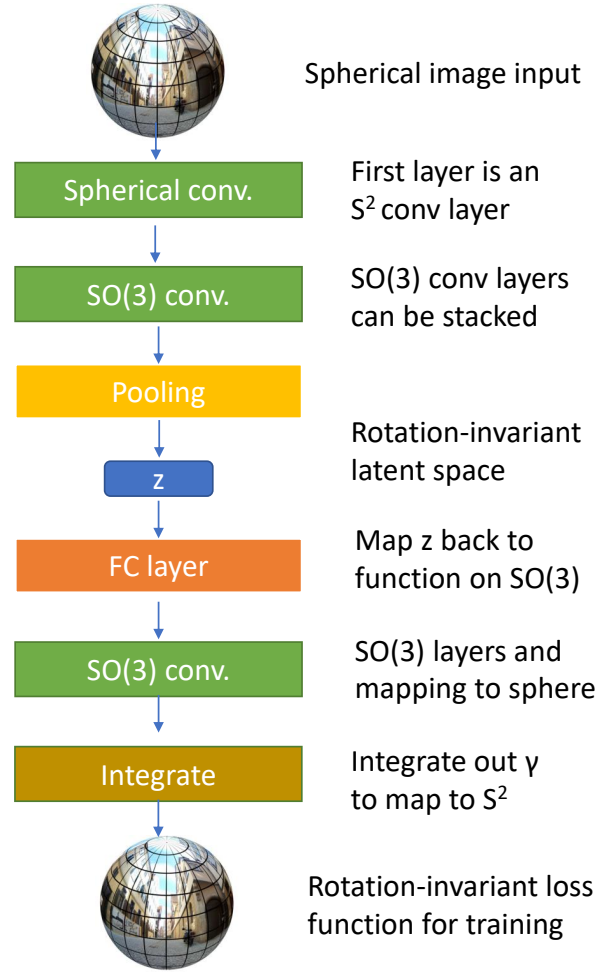


Figure 1: The figure provides an overview of the proposed rotation-invariant autoencoder for spherical images. The encoder consists of an S^2 convolutional layer followed by a series of $SO(3)$ convolutional layers, and finally the pooling layer which creates a rotation-invariant representation. We can either use this as the encoder output (as in the figure) or use further layers in the encoder to get the output \mathbf{z} . The decoder first maps \mathbf{z} to a function on $SO(3)$, using a fully connected layer. This is followed by a stack of $SO(3)$ convolutional layers where all the feature maps are still functions on $SO(3)$. Finally, we use an integration layer to integrate out one of the angles to form a function on S^2 which is also the output of the rotation-invariant autoencoder. This framework is trained using the rotation-invariant loss function proposed in this paper.

The filters in the various S^2 and $SO(3)$ convolutional layers are the trainable parameters in the autoencoders, for which we have to design a novel loss function.

4.3. Rotation-invariant loss function

The latent space of the autoencoder is, by design, invariant to 3D rotations of the input spherical images. However, this also means that all the information about the rotation is discarded, and hence the *reconstruction error can only be measured up to an unknown 3D rotation*. To this end, we use the following function

$$L(f, \hat{f}) = \int_{S^2} |f(x)|^2 dx + \int_{S^2} |\hat{f}(x)|^2 dx - 2 \max_{SO(3)} \{(f \star \hat{f})\}, \tag{10}$$

where the max operator is over the $SO(3)$ function that is the output of the spherical cross-correlation function \star . Essentially, the function finds the best rotation $R \in SO(3)$ such that the difference between $f(R^{-1}x)$ and $\hat{f}(x)$. Clearly, the loss function is also rotation-invariant, as it solves for the optimal alignment before computing the usual squared error loss. While training the network, we compute this loss over a mini-batch and average it, as is normally done. We can employ the Fourier correlation theorem to compute the above spherical cross-correlation efficiently.

5. Experimental results

We conduct extensive experiments on the proposed rotation-invariant autoencoder using publicly available datasets. We show that compared to a vanilla autoencoder trained without using the proposed loss function, the proposed framework is significantly better in terms of reconstruction performance, as well as clustering and classification metrics.

5.1. Spherical MNIST

Dataset details: MNIST is a commonly used dataset [26] in computer vision research consisting of handwritten images of digits 0-9. Here, we use a spherical version of MNIST, called spherical MNIST, by Cohen et al. [5]. Using stereographic projection, all the digits are projected onto the northern hemisphere of a unit sphere. There are two versions of the dataset – (a) NR: all the digits on the sphere are aligned, i.e. they have the same orientation and (b) R: after projection onto the sphere, the spherical images are rotated randomly. Each of these datasets consists of 60000 training and 10000 test examples. Note that the bandwidth of the signals is set to $b = 30$. This means that the size of the spherical signal is 60×60 , i.e., the spherical signal is sampled at 60 values of $\alpha \in [0, 2\pi]$ and $\beta \in [0, \pi]$ using the Driscoll-Healy grid [8].

Autoencoder architecture and training details: The first layer of the encoder consists of an S^2 convolutional layer with 20 output channels and it reduces the bandwidth

Train/test setting	Vanilla AE (L2 loss)	Proposed AE Rotation-invariant loss
NR/NR	18.24	22.46
R/R	10.35	22.52
NR/R	14.33	22.41

Table 1: Reconstruction results on Spherical MNIST, in terms of PSNR (dB), for different settings and variants of spherical autoencoders. We see that the proposed method outperforms the vanilla AE for all settings. We also observe that the proposed framework yield stable performance over all the settings as expected, as the latent representations are exactly rotation-invariant.

to $b = 12$. This is followed by a $SO(3)$ convolutional layer with 40 output channels which further reduces the bandwidth of the feature maps to 6. Both these layers utilize element-wise ReLU non-linearities as the activation function. As shown in Figure 1, we then use the pooling layer defined in Equation (8) to create the rotation invariant representation. For most of the experiments, we set the latent dimension, $dim(\mathbf{z}) = 120$. In the decoder, we use a fully connected layer to map \mathbf{z} to a function on $SO(3)$ with $b = 6$. This is followed by 2 $SO(3)$ convolutional layers which upsample the bandwidth to 12 and 30. The integration layer is used to produce the reconstructed image on the sphere. We train two types of networks – (a) Vanilla AE (the baseline) Here, the spherical autoencoder trained using the regular L2 loss given by $L_{euc}(f, \hat{f}) = \|f - \hat{f}\|_2^2$ and (b) Rotation-invariant AE trained using the proposed rotation-invariant loss function. These networks are trained for three different settings – (a) Train NR/Test NR: both the training and test sets are aligned and have the same orientation (b) Train R/Test R: Both the train and test set have random rotations applied to them and (c) Train NR/Test R: The training set is aligned while the test set has random rotations applied to it. That is, in this setting, the trained network is subject to unseen rotations at test time, and is the most challenging setting. The autoencoders are trained for 20 epochs using Adam optimizer [17] with an initial learning rate of 0.1 and a batch size of 32.

Results: We conduct three sets of experiments on this dataset for the different settings described above. First, we compare the various methods based on the reconstruction peak signal-to-noise ratio (PSNR) between the input spherical image and the reconstructed image for all the examples in the test set. The results are shown in Table 2. We clearly see that the proposed autoencoder trained using the rotation-invariant loss function outperforms the vanilla autoencoder, trained with just the L2 loss, for all cases. It is especially important to note that, compared to Train NR/Test

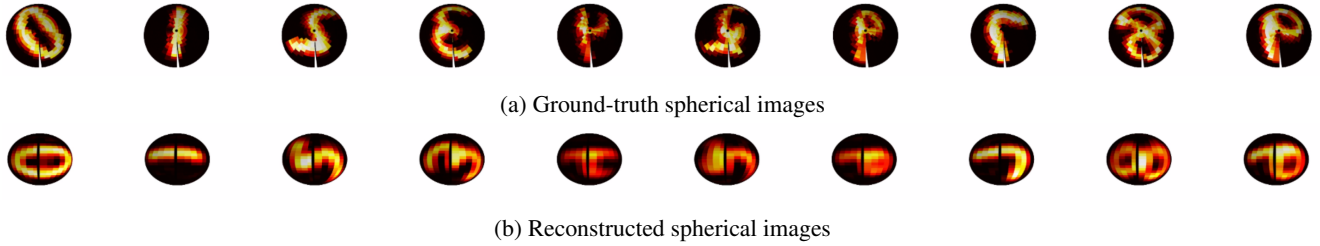


Figure 2: Visualization of the ground-truth spherical images (a) which are also the input to the autoencoder and the reconstructed images (b) from the proposed rotation-invariant autoencoder trained using the rotation-invariant loss function. Note that due to rotation-invariance in the latent space, the reconstruction can be achieved only up to a 3D rotation, as seen in the figure. The spherical images have been partially aligned for easier visualization.

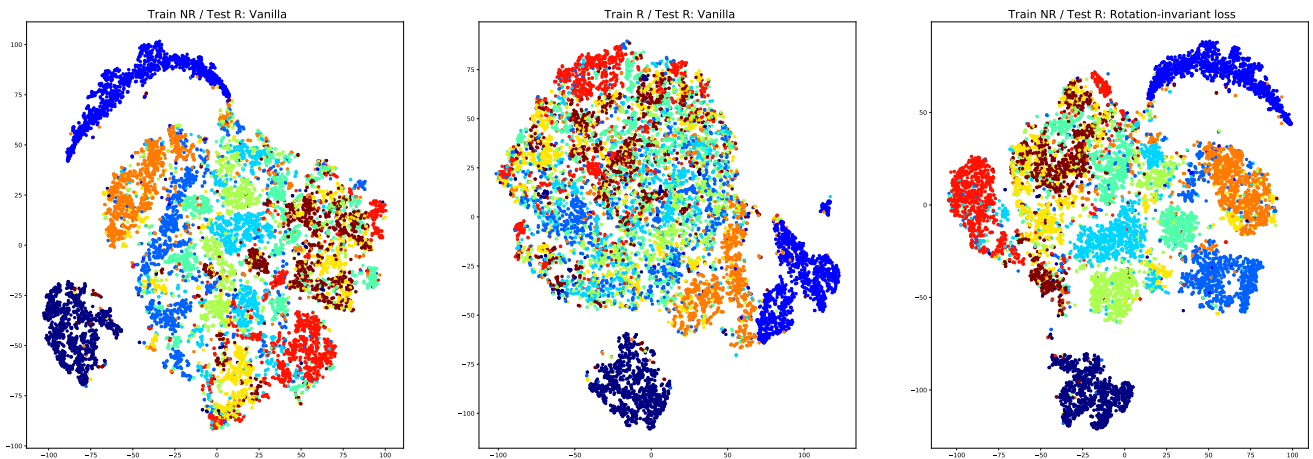


Figure 3: t-SNE visualization of latent features obtained from different spherical autoencoder variants we trained on Spherical MNIST for our experiments. Legend: dark blue = 0, blue = 1, light blue = 2, cyan = 3, dark green = 4, light green = 5, yellow = 6, orange = 7, red = 8, brown = 9. As expected, we see a significant overlap between the points for '6' and '9'.

NR for the case of Train NR/Test R, the vanilla autoencoder (trained with the L2 loss) completely fails, while rotation-invariant autoencoder’s performance is not affected.

Second, we gather the latent features for both the train and test images for the various settings using both the vanilla and the proposed rotation-invariant autoencoder. Then, we train a simple multi-class linear classifier using a single fully-connected layer to map from the 120-dimensional latent feature to a probability distribution over the 10 classes. We measure the classification accuracy on the held out test set. As shown in Table 2, we can see that the proposed framework is significantly better than the vanilla spherical autoencoder. We also compare our method with the purely supervised approach of Cohen et al. [5]. For this, we construct a deeper spherical CNN classifier with a S^2 convolutional layer followed by a $SO(3)$ convolutional layer, the pooling layer and a fully connected layer. We

observe that the features obtained by unsupervised learning actually have a significant amount of discriminative information and perform only a little worse than the fully supervised technique. We also conduct a few-shot learning experiment to better illustrate the advantage of unsupervised feature learning. We see from Table 4 that when we have very few labeled examples for training classifiers, using the latent features of the proposed rotation-invariant autoencoder outperforms the supervised deep spherical CNN.

Third, we use the latent features for the various cases and perform both 2D visualization of the latent features using t-SNE [28] as well as k -means clustering with $k = 10$. The t-SNE plots are shown in Figure 3, which show that the clusters are clearly more compact and homogeneous for the proposed method, compared to the vanilla autoencoder. Using the clusters from the k -means algorithm, we compute common clustering metrics – purity, homogeneity and

Method	Purity	Homogeneity	Completeness	Classification Accuracy (%)
Vanilla AE Train NR/Test R	0.37	0.27	0.29	86.58
Vanilla AE Train R/Test R	0.35	0.25	0.27	74.37
Rotation-invariant AE (proposed) Train NR/Test R	0.40	0.39	0.31	89.42

Table 2: Clustering and classification results on Spherical MNIST. Clearly, the proposed method outperforms the other unsupervised baselines in all metrics. By comparison, our implementation of S^2 CNN (described in the text) [5], which is a fully supervised deep classifier, yields 94% classification accuracy.

$dim(\mathbf{z})$	Vanilla AE Train NR/Test NR	Vanilla AE Train R/Test R	Rot-inv AE Train NR/Test R
60	17.45	10.36	22.46
120	18.24	10.33	22.55
240	18.03	10.38	22.41

Table 3: Effect of dimension of the latent space measured in terms of PSNR (dB) on the test set. We see that the performance is quite stable with respect to $dim(\mathbf{z})$ and using 120 dimensions yields the best results.

Percentage of examples labeled	Deep S^2 CNN (fully supervised)	Rot-inv AE features (unsupervised)
1	33.90%	63.73%
2	62.74%	69.28%
5	80.82%	74.76%
10	86.32%	79.71%
100	95.74%	89.42%

Table 4: Classification accuracy on the test set with few-shot learning. When there are few labeled examples, the unsupervised features can outperform the fully supervised deep S^2 CNN.

completeness for the latent features and report them in Table 2, where we observe improved performance using the proposed method.

Effect of latent dimension In order to study the effect of the dimension of the latent space, we train autoencoders for the various settings with $dim(\mathbf{z}) = 60, 120, 240$ and record the reconstruction PSNRs on the test set. The results thus obtained are shown in Table 3.

5.2. SHREC17 shape retrieval

Dataset details: The dataset consists [35] of 51300 3D meshes belonging to 55 classes such as chairs, tables and airplanes. For the experiments, we use the variant of the dataset where both the training and test set are randomly rotated. The 3D meshes are centered at the origin and are projected onto a sphere around the mesh using ray casting.

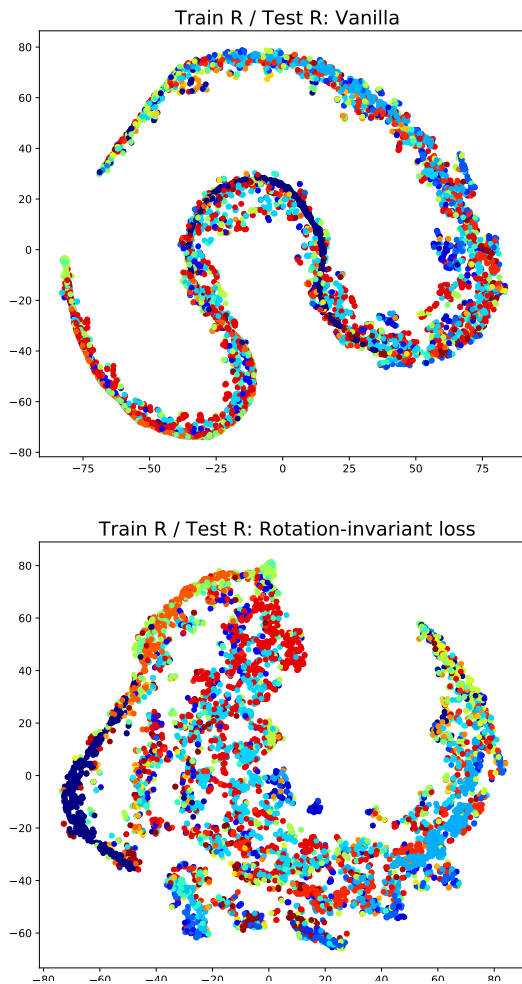


Figure 4: t-SNE visualization of latent features for the SHREC17 dataset. The clusters are more easily visible using the proposed method.

Rays are cast from the origin passing through the mesh and hitting the sphere. The distance between the point on the mesh and the sphere is recorded as the signal on the sphere, and forms the spherical representation of the 3D mesh. As before Driscoll-Healy grid is used to sample the sphere with a bandwidth $b = 30$, i.e. the spherical signals can be stored as 60×60 arrays.

Method	Purity	Homogeneity	Completeness	Classification Accuracy (%)
Vanilla AE	0.30	0.26	0.22	48.80
Rotation-invariant AE (proposed)	0.41	0.38	0.31	57.76

Table 5: Clustering and classification results on SHREC17. Clearly, the proposed method outperforms the other unsupervised baselines in all metrics. By comparison, our implementation of S^2 CNN (with 3 conv layer) [5], which is a fully supervised deep classifier, yields 65.42% classification accuracy.

Type	Method	P@N	R@N	F1@N	mAP	NDCG
Supervised	Tatsuma_ReVGG	0.705	0.769	0.719	0.696	0.783
	Furuya_DLAN	0.814	0.683	0.706	0.656	0.754
	SHREC16-Bai_GIFT	0.678	0.667	0.661	0.607	0.735
	Deng_CM-VGG5-6DB	0.412	0.706	0.472	0.524	0.624
	S^2 CNN [5]	0.701	0.711	0.699	0.676	0.756
Unsupervised	Vanilla AE	0.075	0.092	0.066	0.008	0.064
	Rotation-invariant AE (proposed)	0.351	0.361	0.335	0.215	0.345

Table 6: Shape retrieval results on SHREC17 compared to fully supervised methods. We see that even the unsupervised features obtained using our proposed method with the rotation-invariant loss function yields good results, especially when compared to the vanilla spherical autoencoder with the L2 loss function. The results for the supervised methods are taken from [5].

Autoencoder architecture and training details: Both the autoencoder architecture and the hyperparameters are the same as in the case of the Spherical MNIST dataset. As before, the latent space is 120-dimensional and invariant to 3D rotations applied at the input. As before, we train a vanilla spherical autoencoder trained using a simple L2 loss function and the proposed autoencoder framework trained using the rotation-invariant loss function.

Results: We conduct three set of experiments on this dataset. First, we compute the latent features for both the training and test set 3D shape spherical representations. The latent features are then used to train a simple linear classifier. The results are shown in Table 5. We see that the proposed framework yields significantly higher classification accuracy, compared to vanilla AE. Second, as in the case of Spherical MNIST, we conduct similar clustering experiments by performing k -means clustering with $k = 55$. We report commonly used clustering metrics – purity, homogeneity and completeness – in Table 5. We can clearly observe improved performance with the proposed method, compared to the vanilla AE trained with L2 loss. Third, we conduct shape retrieval on the held out test set following the protocol in [35]. The results are reported in Table 6 for various retrieval metrics and comparison with fully supervised methods is also provided. We observe that the features obtained through the proposed method work reasonably well for shape retrieval.

6. Conclusion

In this paper, we presented a novel architecture for learning rotation-invariant representations for spherical images in an unsupervised fashion. We designed an autoencoder using S^2 and $SO(3)$ convolutional layers, which are equivariant to 3D rotations and the latent space is constrained to be rotation-invariant using a pooling layer. We proposed a rotation-invariant loss function based on the maximum of spherical cross-correlation in order to train such networks. Through experiments on multiple datasets of spherical images and spherical representations of 3D shapes, we showed the utility of such representations. The proposed method results in good performance in terms of clustering, retrieval and classification based on unsupervised learning. We hope that this work will lead to similar transformation-invariant unsupervised feature learning methods for other transformations such as scale, affine transforms etc. and for other domains such as images, graphs and sets.

References

- [1] Panos Achlioptas, Olga Diamanti, Ioannis Mitliagkas, and Leonidas Guibas. Learning representations and generative models for 3d point clouds. In *International conference on machine learning*, pages 40–49. PMLR, 2018. 2
- [2] Martin Arjovsky, Léon Bottou, Ishaan Gulrajani, and David Lopez-Paz. Invariant risk minimization. *arXiv preprint arXiv:1907.02893*, 2019. 2

- [3] Taco Cohen, Maurice Weiler, Berkay Kicanaoglu, and Max Welling. Gauge equivariant convolutional networks and the icosahedral cnn. In *ICML*, 2019. 2
- [4] Taco Cohen and Max Welling. Group equivariant convolutional networks. In *International conference on machine learning*, pages 2990–2999, 2016. 2
- [5] Taco S Cohen, Mario Geiger, Jonas Köhler, and Max Welling. Spherical cnns. *International Conference on Learning Representations*, 2018. 1, 2, 3, 4, 5, 6, 7, 8
- [6] Pim de Haan, Maurice Weiler, Taco Cohen, and Max Welling. Gauge equivariant mesh cnns: Anisotropic convolutions on geometric graphs. *arXiv preprint arXiv:2003.05425*, 2020. 2
- [7] Samuel Dodge and Lina Karam. Understanding how image quality affects deep neural networks. In *2016 eighth international conference on quality of multimedia experience (QoMEX)*, pages 1–6. IEEE, 2016. 2
- [8] James R Driscoll and Dennis M Healy. Computing fourier transforms and convolutions on the 2-sphere. *Advances in applied mathematics*, 15(2):202–250, 1994. 5
- [9] Carlos Esteves. Theoretical aspects of group equivariant neural networks. *arXiv preprint arXiv:2004.05154*, 2020. 3
- [10] Carlos Esteves, Christine Allen-Blanchette, Ameesh Makadia, and Kostas Daniilidis. Learning so (3) equivariant representations with spherical cnns. In *Proceedings of the European Conference on Computer Vision (ECCV)*, pages 52–68, 2018. 1, 2, 3
- [11] Carlos Esteves, Ameesh Makadia, and Kostas Daniilidis. Spin-weighted spherical cnns. *Advances in Neural Information Processing Systems*, 33, 2020. 2
- [12] Robert Geirhos, Jörn-Henrik Jacobsen, Claudio Michaelis, Richard Zemel, Wieland Brendel, Matthias Bethge, and Felix A Wichmann. Shortcut learning in deep neural networks. *arXiv preprint arXiv:2004.07780*, 2020. 2
- [13] Joshua Gluckman and Shree K Nayar. Ego-motion and omnidirectional cameras. In *Sixth International Conference on Computer Vision (IEEE Cat. No. 98CH36271)*, pages 999–1005. IEEE, 1998. 1
- [14] Ian Goodfellow, Honglak Lee, Quoc Le, Andrew Saxe, and Andrew Ng. Measuring invariances in deep networks. *Advances in neural information processing systems*, 22:646–654, 2009. 2
- [15] Geoffrey E Hinton, Alex Krizhevsky, and Sida D Wang. Transforming auto-encoders. In *International conference on artificial neural networks*, pages 44–51. Springer, 2011. 2
- [16] Max Jaderberg, Karen Simonyan, Andrew Zisserman, et al. Spatial transformer networks. In *Advances in neural information processing systems*, pages 2017–2025, 2015. 2
- [17] Diederik P Kingma and Jimmy Ba. Adam: A method for stochastic optimization. *International Conference on Learning Representations*, 2015. 5
- [18] Risi Kondor, Zhen Lin, and Shubhendu Trivedi. Clebsch-gordan nets: a fully fourier space spherical convolutional neural network. In *Advances in Neural Information Processing Systems*, pages 10117–10126, 2018. 2, 3
- [19] Risi Kondor, Hy Truong Son, Horace Pan, Brandon Anderson, and Shubhendu Trivedi. Covariant compositional networks for learning graphs. *arXiv preprint arXiv:1801.02144*, 2018. 2
- [20] Risi Kondor and Shubhendu Trivedi. On the generalization of equivariance and convolution in neural networks to the action of compact groups. In *International Conference on Machine Learning*, pages 2747–2755, 2018. 2
- [21] Kaushik Koneripalli, Suhas Lohit, Rushil Anirudh, and Pavan Turaga. Rate-invariant autoencoding of time-series. In *ICASSP 2020-2020 IEEE International Conference on Acoustics, Speech and Signal Processing (ICASSP)*, pages 3732–3736. IEEE, 2020. 2
- [22] Peter Kostelec and Daniel Rockmore. Soft: So(3) fourier transforms. 2007. 2
- [23] Alex Krizhevsky, Ilya Sutskever, and Geoffrey E Hinton. Imagenet classification with deep convolutional neural networks. *Neural Information Processing Systems*, 2012. 2
- [24] Tejas D Kulkarni, William F Whitney, Pushmeet Kohli, and Josh Tenenbaum. Deep convolutional inverse graphics network. In *Advances in neural information processing systems*, pages 2539–2547, 2015. 2
- [25] Denis Kuzminykh, Daniil Polykovskiy, and Alexander Zhebrak. Extracting invariant features from images using an equivariant autoencoder. In *Asian Conference on Machine Learning*, pages 438–453, 2018. 2
- [26] Yann LeCun. The mnist database of handwritten digits. <http://yann.lecun.com/exdb/mnist/>. 5
- [27] Suhas Lohit, Qiao Wang, and Pavan Turaga. Temporal transformer networks: Joint learning of invariant and discriminative time warping. In *Proceedings of the IEEE Conference on Computer Vision and Pattern Recognition*, pages 12426–12435, 2019. 2
- [28] Laurens van der Maaten and Geoffrey Hinton. Visualizing data using t-sne. *Journal of machine learning research*, 9(Nov):2579–2605, 2008. 6
- [29] Haggai Maron, Heli Ben-Hamu, Nadav Shamir, and Yaron Lipman. Invariant and equivariant graph networks. In *International Conference on Learning Representations*, 2018. 2
- [30] Haggai Maron, Or Litany, Gal Chechik, and Ethan Fetaya. On learning sets of symmetric elements. *International Conference on Machine Learning*, 2020. 2
- [31] Shinji Morita, Kazumasa Yamazawa, and Naokazu Yokoya. Networked video surveillance using multiple omnidirectional cameras. In *Proceedings 2003 IEEE International Symposium on Computational Intelligence in Robotics and Automation. Computational Intelligence in Robotics and Automation for the New Millennium (Cat. No. 03EX694)*, volume 3, pages 1245–1250. IEEE, 2003. 1
- [32] Luis Payá, Arturo Gil, and Oscar Reinoso. A state-of-the-art review on mapping and localization of mobile robots using omnidirectional vision sensors. *Journal of Sensors*, 2017. 1
- [33] Siamak Ravanbakhsh, Jeff Schneider, and Barnabas Poczos. Deep learning with sets and point clouds. *International Conference on Learning Representations - Workshop track*, 2017. 2
- [34] Sara Sabour, Nicholas Frosst, and Geoffrey E Hinton. Dynamic routing between capsules. In *Advances in neural information processing systems*, pages 3856–3866, 2017. 2

- [35] Manolis Savva, Fisher Yu, Hao Su, Song Bai, Xiang Bai, et al. Shrec16 track: largescale 3d shape retrieval from shapenet core55. In *Eurographics Workshop on 3D Object Retrieval*, 2017. 7, 8
- [36] Zhixin Shu, Mihir Sahasrabudhe, Riza Alp Guler, Dimitris Samaras, Nikos Paragios, and Iasonas Kokkinos. Deforming autoencoders: Unsupervised disentangling of shape and appearance. In *Proceedings of the European conference on computer vision (ECCV)*, pages 650–665, 2018. 2
- [37] Ankita Shukla, Sarthak Bhagat, Shagun Uppal, Saket Anand, and Pavan Turaga. Product of orthogonal spheres parameterization for disentangled representation learning. *British Machine Vision Conference*, 2019. 2
- [38] Erik Henning Thiede, Truong Son Hy, and Risi Kondor. The general theory of permutation equivariant neural networks and higher order graph variational encoders. *arXiv preprint arXiv:2004.03990*, 2020. 2
- [39] Maurice Weiler, Fred A Hamprecht, and Martin Storath. Learning steerable filters for rotation equivariant cnns. In *Proceedings of the IEEE Conference on Computer Vision and Pattern Recognition*, pages 849–858, 2018. 2
- [40] Daniel Worrall and Max Welling. Deep scale-spaces: Equivariance over scale. In *Advances in Neural Information Processing Systems*, pages 7366–7378, 2019. 2
- [41] Daniel E Worrall, Stephan J Garbin, Daniyar Turmukhambetov, and Gabriel J Brostow. Harmonic networks: Deep translation and rotation equivariance. In *Proceedings of the IEEE Conference on Computer Vision and Pattern Recognition*, pages 5028–5037, 2017. 2
- [42] Wenju Xu, Guanghui Wang, Alan Sullivan, and Ziming Zhang. Towards learning affine-invariant representations via data-efficient cnns. In *The IEEE Winter Conference on Applications of Computer Vision*, pages 904–913, 2020. 2
- [43] Yichong Xu, Tianjun Xiao, Jiaying Zhang, Kuiyuan Yang, and Zheng Zhang. Scale-invariant convolutional neural networks. *arXiv preprint arXiv:1411.6369*, 2014. 2
- [44] Yasushi Yagi. Omnidirectional sensing and its applications. *IEICE transactions on information and systems*, 82(3):568–579, 1999. 1
- [45] Yaoqing Yang, Chen Feng, Yiru Shen, and Dong Tian. Foldingnet: Point cloud auto-encoder via deep grid deformation. In *Proceedings of the IEEE Conference on Computer Vision and Pattern Recognition*, pages 206–215, 2018. 2
- [46] Manzil Zaheer, Satwik Kottur, Siamak Ravanbakhsh, Barnabas Poczos, Russ R Salakhutdinov, and Alexander J Smola. Deep sets. In *Advances in neural information processing systems*, pages 3391–3401, 2017. 2
- [47] Binbin Zhang, Wen Shen, Shikun Huang, Zhihua Wei, and Quanshi Zhang. 3d-rotation-equivariant quaternion neural networks. *European Conference on Computer Vision*, 2020. 2